Relationships Between Cluster Secondary Ion Mass Intensities Generated by Different Cluster Primary Ions

Martin P. Seah, Felicia M. Green, and Ian S. Gilmore
Quality of Life Division, National Physical Laboratory, Teddington, Middlesex, United Kingdom

Measurements are described to evaluate the constitution of secondary ion mass spectra for both monatomic and cluster primary ions. Previous work shows that spectra for different primary ions may be accurately described as the product of three material-dependent component spectra, two being raised to increasing powers as the cluster size increases. That work was for an organic material and, here, this is extended to $(SiO_2)_tOH^-$ clusters from silicon oxide sputtered by 25 keV Bi_n^+ cluster primary ions for $n = 1$, 3, and 5 and $1 \le t \le 15$. These results are described to a standard deviation of 2.4% over 6 decades of intensity by the product of a constant with a spectrum, $\mathbf{H}^*_{SiOH}$, and a power law spectrum in t. This evaluation is extended, using published data for Si_t^+ sputtered from Si by 9 and 18 keV Au^- and Au_3^-, with confirmation that the spectra are closely described by the product of a constant with a spectrum, $\mathbf{H}^*_{Si}$, and a simple spectrum that is an exponential dependence on t, both being raised to appropriate powers. This is confirmed with further published data for 6, 9, 12, and 18 keV Al^- and Al_2^- primary cluster ions. In all cases, the major effect of intensity is then related to the deposited energy of the primary ion at the surface. The constitution of SIMS spectra, for monatomic and cluster primary ion sources, is shown, in all cases, to be consistent with the product of a constant with two component spectra raised to given powers. (J Am Soc Mass Spectrom 2010, 21, 370–377) © 2010 American Society for Mass Spectrometry

The analysis of complex molecules in SIMS has been enhanced in recent years by the application of primary cluster ions of the type $Au_n^{\pm}$, Bi_n^+, C_{60}^{n+}, etc. These provide significantly higher yields of the larger fragments that are important in the analysis of larger molecules. Over the years, there has not been a great focus on the relative intensities of the many secondary ions in the spectrum and their changes with the change in primary ion cluster size and energy. Analysts have usually focused on the enhancement of intensity of a particular characteristic ion obtained when using larger cluster primary ions. However, the fragment ions in the spectrum can be used to construct the structure of the molecules or the arrangement of atoms at a surface as well as provide important data as a function of depth in depth profiles [1–8]. Studies of the whole secondary ion spectrum and its evolution from one primary ion source to another are an important part of the infrastructure to the whole field of secondary ion mass spectrometry.

Much historical data and data in spectral libraries [9–11] are for inert gas primary ions. Over the years, the primary ion sources used have changed and changed again. Different spectrometer manufacturers fit different primary ion sources. It is important, therefore, if analysts are to make the best use of their instruments and of the published literature and data sources, that the relationships for the secondary ion spectra from different primary ion sources is characterized and understood.

Elsewhere, we have studied the secondary ion mass spectrum from organic materials in detail for a number of primary ions and have proposed that the spectra are all related accurately to one another by three sample-related component spectra with the observed spectrum being a product, not a sum, of those component spectra [12]. It is important to understand if this is a generic effect in SIMS or if it is limited, in some way, to organic materials. One of the major sets of work on the intensities of many secondary ions as a function of cluster primary ion size is the study of the sputtering of elemental solids by Belykh and coworkers [13–19]. These studies show the relative intensities of fragments such as $M_t^{\pm}$, where $1 \le t \le 20$ for the sputtering of M = Nb, Si, and Ta.

One of the main purposes of Belykh and coworkers studies was to characterize and investigate the non-additivity of cluster sputtering as compared with monatomic sputtering. These analyses involve the evaluation of an enhancement factor $K_{n,1}$ where

Address reprint requests to Dr. F. M. Green, Quality of Life Division, National Physical Laboratory, Hampton Road, Teddington TW11 0LW, UK.
E-mail: felicia.green@npl.co.uk

1044-0305/10/$32.00
doi:10.1016/j.jasms.2009.10.021

Published online November 5, 2009
Received August 28, 2009
Revised October 27, 2009
Accepted October 30, 2009

$$K_{n,1} = \frac{Y_n(E)}{nY_1(E/n)} \quad (1)$$

and where $Y_n(E)$ is the yield of a particular species from the impact of primary ion clusters of n atoms with total energy E, and $Y_1(E)$ is the yield of that species for monatomic primary ions with energy E/n. In this equation, if the yield for a primary ion cluster was n times the yield for each separate impacting atom of the cluster at the same velocity, then $K_{n,1}$ would be unity. That $K_{n,1}$ was always above unity showed that the sputtering was a nonlinear function of the energy deposited at the surface when clusters were involved, and this was interpreted in terms of spike formation [13]. The present work does not change that general view. Results for the Au_n^- sputtering of Ta [14, 15] for $1 \leq n \leq 3$ showed that the yield of clusters Ta_t^+ $5 \leq t \leq 12$ exhibited an intensity dependence that fitted an exponential form

$$Y_{n,t} = A_n \exp(-s_n t) \quad (2)$$

where s_n decreased as n increased. For $t < 5$, the dependence was more complex. This led to $K_{n,1}$ values that rose approximately linearly with t, reaching a factor of 1000 at $t = 10$. This was interpreted to show an anomalously high non-additivity of sputtering by the gold clusters. Very similar results were observed for Nb [16], Si [17], and V [18] sputtered by Au_n^- clusters and for Si sputtered by Al_n^- clusters [19]. Baudin et al. [20] also show results following this exponential law for $t > 3$ for C_t^- sputtered from carbon foils by 20 MeV C_{60}^+ primary ions both in transmission and reflection.

However, in more recent work, Samartsev and Wucher [21] show results that follow the power law relation

$$Y_{n,t} = B_n t^{-b_n} \quad (3)$$

for neutral secondary In_t clusters sputtered from In by 5 keV and 10 keV Au^-, Au_2^-, Au_3^- and Au_5^- primary ions. They note that the predictions of Belykh et al. [22] are at variance with this result. In all cases, the parameters b_n and s_n change monotonically such that both the relative quantities of the larger fragments and $K_{n,1}$ increase as the primary ion cluster size, n, increases.

Others who have found results following eq 3 are Coon et al. [23] for secondary neutral Cu_t sputtered from Cu by 3.9 keV Ne^+, Ar^+ and Xe^+ primary ions, Colla et al. [24] for Cu_t similarly by 5 keV Ar^+, Staudt, Heinrich, and Wucher [25] for secondary neutral Ag_t clusters sputtered from Ag by 15 keV Xe^+ primary ions and Samartsev and Wucher [26] for secondary neutral In_t clusters sputtered from In by Au_n^- primary ions. King et al. [27], using 15 keV Ar^+, also find the power law valid for $t < 10$ for secondary neutral Ni_t and Al_t clusters sputtered from the pure metals, and for $Al_{t-m}Ni_m$ clusters sputtered from an NiAl single crystal. In these studies, the ionization probability rises with the secondary cluster size t in an approximate power law, so that the dependence for ions is weaker but is still a power law.

Staudt and Wucher [28] extend the above work to show that, when corrected for detector efficiency, a change in the power occurs between the range $1 \leq t \leq 10$ and the range $10 \leq t \leq 100$. It is known that the efficiency of the secondary ion detection reduces as the energy per constituent atom reduces [29]. Thus, the measured detection efficiency, whilst close to unity for low masses, reduces more and more as t rises. The mass at which the efficiency starts to fall depends on the particle velocity at the detector electrode and hence on the accelerating voltage into the detector. This could make a relation like eq 3 move towards eq 2 but is unlikely to change the underlying function to an exponential since, in the limit, the detector term is also of a power law form. It is not known if the detector efficiency has been a significant issue in the past but, to avoid it here, a high detector energy of 20 keV has been used [29].

Staudt and Wucher [28] note that a summary of their data for many elemental metal systems shows $4 < b_n < 9$ with many results in the range 6 to 8. They also note that the only model calculations predicting power law cluster yield distributions are based on the shock wave theory of Bitensky and Parilis [30] and the thermodynamic expansion through a liquid/gas coexistence regime theory of Urbassek [31]. These theories give $b_n = 2$ and $2^{1/3}$, respectively, and are significantly lower than the values found by experiment. Note, however, that in Urbassek's theory [31], there is a second multiplying term that depends exponentially on the energy needed to release the cluster from the bulk and this, depending on t, may make up for the difference between the $2^{1/3}$ and the experimental data. Yamamoto et al. [32] show the power law of eq (3) to be valid for 4 keV Ar^+, Xe^+, and SF_5^+ primary ions sputtering C_t^- secondary ions from diamond for $1 \leq t \leq 10$, with $1.8 < b_n < 4.7$, and Brunelle et al. [33] show that eq 3 is also valid for Au_4^+ primary ions sputtering negative secondary ions from CsI using 37.5 keV/atom and 5.04 MeV/atom primary ions with $b_n = 1.6$ and 2.3, respectively. In this latter case, secondary ion molecular fragments $(CsI)_tI^-$ were analyzed for $1 \leq t \leq 12$. That the alkali halides, in general show power law spectra for 4 keV Ar^+ and Xe^+ primary ions was first shown by Barlak et al. [34, 35].

All these results, whether exponential or power law, show enhanced emission of the larger secondary ions as the deposited energy density rises, as expected for a thermal spike, although the precise dependence from theory is not yet clear. Elsewhere [12], we show that for Bi_n^+ primary ions, the spectra, $I(Bi_n^+)$, for the cluster sputtering of the organic molecule, Irganox 1010, in the static SIMS limit [36] may be predicted very accurately from the spectrum for argon, $I(Ar^+)$, using the relation

$$I(\mathrm{Bi}_n^+) = I(\mathrm{Ar}^+)\,(\mathbf{L}^*_{\mathrm{Irg}})^{a_n}\,(\mathbf{H}^*_{\mathrm{Irg}})^{b_n} \quad (4)$$

where $\mathbf{L}^*_{\mathrm{Irg}}$ and $\mathbf{H}^*_{\mathrm{Irg}}$ are two spectra, each of 389 mass channels, reflecting internal processes, and a_n and b_n are constants that depend on n. In eq 4, the I(X) may be taken either as the yields (i.e., the spectrum per incident ion) or the intensity in a spectrum where the number of incident primary ions is the same in all spectra. In our earlier work [12], $\mathbf{L}^*_{\mathrm{Irg}}$ and $\mathbf{H}^*_{\mathrm{Irg}}$ were originally chosen to emphasize the contributions that led to high and low mass peaks but here we may consider that these two spectra are simply independent spectra with the **H*** and **L*** symbols retained for consistency with that work.

Equation 4 indicates that the differences between spectra concern fragment-dependent scaling factors (i.e., $(\mathbf{L}^*_{\mathrm{Irg}})^{a_n}$ and $(\mathbf{H}^*_{\mathrm{Irg}})^{b_n}$). This describes the enhanced emission of the larger secondary ions, as the deposited energy density rises, very precisely. If eq 4 may be transferred to inorganic and elemental solids, then the $Y_{n,t}$ of eqs 2 or 3 may be treated as spectra and the same effect should be observed. Either eq 2 or eq 3 may be valid for eq 4 to be obeyed. Structure in the divergencies in the data as a function of t, from the smooth dependencies of either eq 2 or eq 3, can be used to test if eq 4 applies to inorganic and elemental solids as well as organics. Inspection of the data of Belykh et al. [19] for Si show a suitable structure in the divergence from a smooth dependence on t, and this is analyzed below. Data for Si are a good test since the low mass of Si ensures that any detector efficiency changes are minimized. Additionally, there are few datasets for secondary ion clusters from compounds and so, here, ion yields of $(SiO_2)_tOH^-$ molecular clusters were measured for a washed, surface oxidized silicon wafer for bombardment by 25 keV Bi^+, Bi_3^+, and Bi_5^+ primary ions. These also show suitable structure for the present study in the divergence from a smooth dependence on t. This compound showed a power law dependence as in eq 3 and as seen in many materials.

Experimental

For the $(SiO_2)_tOH^-$ studies, surface oxidized silicon samples were cleaned by soaking in iso-propyl alcohol (IPA) overnight, followed by 30 s of ultrasonic agitation in IPA and then by argon jet drying. This procedure has been developed to remove as much contamination as possible whilst leaving the surface otherwise unchanged. Other cleaning methods are likely to leave the surface in a different chemical state so that the measured spectra may then be different.

Secondary ion mass spectra were recorded using an ION-TOF time of flight secondary ion mass spectrometer (TOF-SIMS IV), with primary ions of Bi^+, Bi_3^+, and Bi_5^+ at 25 keV. To measure the ion yields, four repeat spectra were averaged, each having been recorded with the same primary ion dose of, typically, 2×10^7 primary ions, on fresh regions, within the static SIMS limit [36]. Primary ion current measurements were recorded by positioning the primary ion beam into a Faraday cup on the sample holder with the current measurement using a calibrated Keithley 6512 electrometer. The impact energy of the secondary ions at the detector was set at 20 keV.

Results and Discussion

For the $(SiO_2)_tOH^-$ studies, the measured yields from the oxidized Si wafer, over six decades of intensity are shown by the large open symbols in Figure 1a. The mass range for the secondary ions up to 1000 u covered $1 \le t \le 15$. We can see that the general trend follows the power law of eq 3) with powers of approximately −5.0,

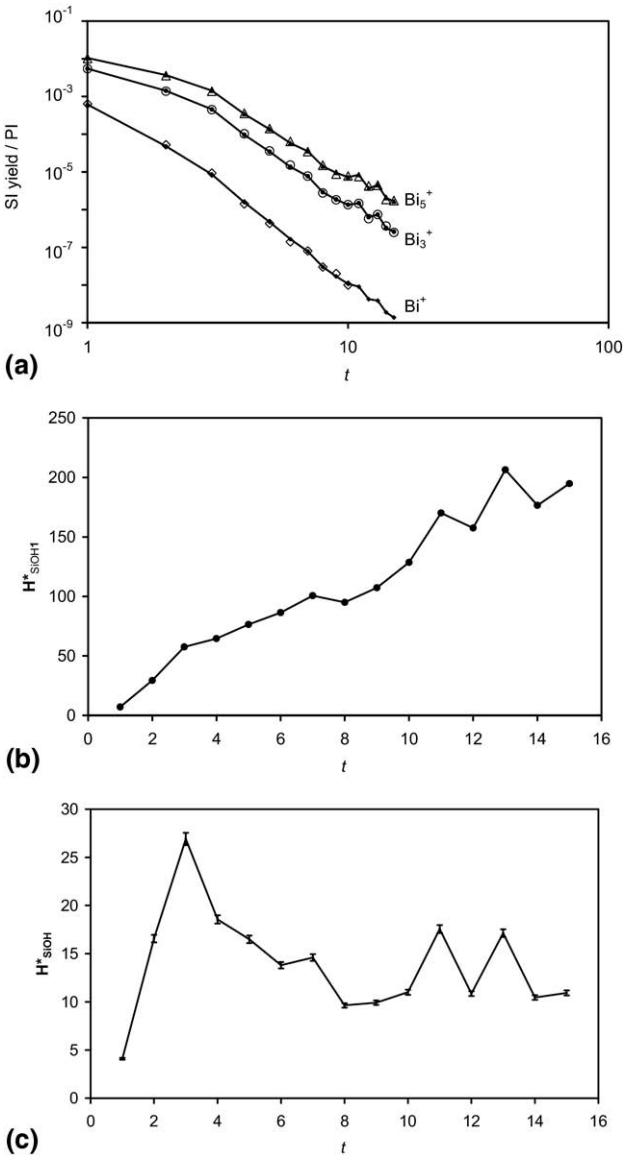

Figure 1. Data for the $(SiO_2)_tOH^-$ secondary ion yield per primary ion for 25 keV Bi^+, Bi_3^+ and Bi_5^+ primary ions, (**a**) experimental data as open symbols and the descriptions of eqs 6, 7, and 8 as the joined small solid symbols, (**b**) $\mathbf{H}^*_{\mathrm{SiOH1}}$, and (**c**) $\mathbf{H}^*_{\mathrm{SiOH}}$ with error bars as standard deviations of 2.4%.

−3.9 and −3.5 for Bi^+, Bi_3^+ and Bi_5^+, respectively, in general agreement with much published work. However, at $t = 1$ and 2, the yields fall significantly below this and, at specific high values of t, the yields may be a factor of 2 away from a simple power law.

We consider the relation

$$I(Bi_n^+) = I(Bi^+)\,(\mathbf{H}^*_{SiOH1})^{b_n} \quad (5)$$

as a first description, and this gives directly the small points linked by the straight lines in Figure 1a. These fit the open symbol data to a relative standard deviation of 2.4%, equivalent to approximately one-tenth of the radius of the plotted open circles. The fit is remarkably good and supports eq 4. The spectrum $\mathbf{H}^*_{SiOH1}$ is shown in Figure 1b. This shows structure that is clear in the Bi_3^+ and Bi_5^+ data but is weak in the Bi^+ data. It also allows us to predict the missing Bi^+ data for $11 \le t \le 15$, where the intensities were weak, as shown in Figure 1a.

Clearly, $I(Bi^+)$ also contains the structure of $\mathbf{H}^*_{SiOH1}$ from Figure 1b so that the data may be further reduced to extract components more clearly. Manipulation of the data does not alter the fit shown in Figure 1a, and this remains with a scatter of 2.4%. $\mathbf{H}^*_{SiOH}$ is constrained to be approximately constant and most of the t dependence is now expressed transparently in a power law term. With this manipulation, we find for the yields

$$I(Bi^+) = (0.0002353)\,(t^{-5.05})\,(\mathbf{H}^*_{SiOH})^{0.68} \quad (6)$$

$$I(Bi_3^+) = (0.001245)\,(t^{-4.06})\,(\mathbf{H}^*_{SiOH})^{1.05} \quad (7)$$

$$I(Bi_5^+) = (0.002381)\,(t^{-3.61})\,(\mathbf{H}^*_{SiOH})^{1.05} \quad (8)$$

where the new $\mathbf{H}^*_{SiOH}$ is like $\mathbf{H}^*_{SiOH1}$ but has had the greater part of the t dependence largely removed. These equations fit the data to the same 2.4% scatter. The new $\mathbf{H}^*_{SiOH}$, with standard uncertainty error bars, is shown in Figure 1c. The power index for t in the second brackets in eq 6 to 9 is rather stronger than that found [33] for $(CsI)_tI^-$, but weaker than for most metals [28]. For each "spectrum," we may write

$$I(Bi_n^+) = F_n\,(\mathbf{L}^*_{SiOH})^{a_n}\,(\mathbf{H}^*_{SiOH})^{b_n} \quad (9)$$

where the F_n are constants and where

$$\mathbf{L}^*_{SiOH} = t^{-1} \quad (10)$$

Clearly, eq 9 describes these $(SiO_2)_tOH^-$ spectra very accurately with the $\mathbf{L}^*_{SiOH}$ spectrum a simple power dependence of the form of eq 3. This does not, of course, prove that eq 2 is incorrect for other systems, since that too conforms to eq 4. It is useful, therefore, to revisit some of the data exhibiting the exponential dependence, and here we have selected the extensive data of Belykh et al. [19] for the sputtering of Si by Au_n^- $1 \le n \le 3$, which represents the elemental system closest to that studied above.

The results of Belykh et al. [19] for sputtering with 9 and 18 keV beams are shown in Figure 2a by the open symbols. Also shown are the fits of the form

$$I_{n,t} = C_n\,[\exp(-s_n t)]\,(\mathbf{H}^*_{Si})^{k_n} \quad (11)$$

where the values of k_n, and s_n are given in Table 1, and where an exponential dependence on t has been used instead of a power law. The values of the constants, C_n, depend on the relative intensity scale chosen by Belykh et al. [19] in their paper. These are not yields but relative yields. The fits for these values are shown by the small points joined by straight lines and exhibit an overall scatter standard deviation of 7% from the experimental data (about half the diameter of the plotted points for the measurements). The result for $t = 13$ is a perfect fit since there is only one data point at that t value and so all higher t values for Au_3^- primary ions will be fit similarly and so are also ignored. So too are yields $<10^{-5}$ of the maximum yield since signal quality is then considered to be too poor. Figure 2b shows the spectrum $\mathbf{H}^*_{Si}$ which, like $\mathbf{H}^*_{SiOH}$ in Figure 1c, is organized to be fairly constant and places most of the t variation into the exponential term. The error bars show the standard uncertainties.

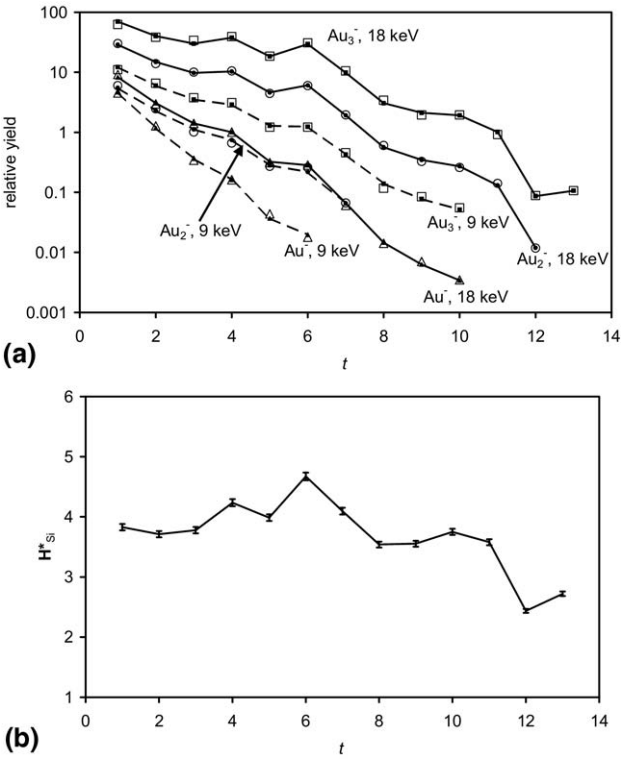

Figure 2. Data for the relative Si_t^+ secondary ion yields, (**a**) experimental data from Belykh et al. [19] normalized to the same Au_n^- primary ion beam currents, as open symbols, and the description of eq 11 as the joined small solid symbols for (——) 18 keV and (---) 9 keV primary ion energy, (**b**) $\mathbf{H}^*_{Si}$ from (**a**) with error bars for a standard deviation of 7%.

Table 1. Values of parameters k_n and s_n for eq (11) for sputtering Si_t^+ by Au_n^- primary ions

Primary ion	Parameter	Energy, keV	
		9	18
Au^-	k_1	3.88	4.55
	s_1	1.248	0.855
Au_2^-	k_2	3.24	4.91
	s_2	0.775	0.506
Au_3^-	k_3	3.55	5.38
	s_3	0.599	0.387

Although one could initially have argued that the data in Figure 2a do not really fit an exponential and that the gradients for some of the data change by a factor of 2 as t increases, the description of eq 11 shows the underlying exponential can be a very accurate description for one of the two component parts for $1 \leq t < 13$. In the spirit of eq 9, here C_n has replaced F_n, s_n has replaced a_n, and $\exp(-t)$ has replaced $\mathbf{L}^*_{Si}$.

Could the data be fitted by replacing $\exp(-t)$ by $1/t$? The answer is, yes, but with a poorer correlation. This requires an $\mathbf{H}^*_{Si}$ with a structure somewhat like Figure 2b but strongly peaked in the centre at $t = 6$. The overall fit equivalent to Figure 1a is now 31% with the values at $t = 1$ significantly in error, with the predictions sometimes being above and sometimes being below the experimental data. If the $t = 1$ data are ignored, the scatter falls to 18%, a result significantly poorer than the 7% when the exponential, $\exp(-t)$, is used as the basis for $\mathbf{L}^*_{Si}$ rather than $1/t$. Note that 18% is just equivalent to the radius of the open points in Figure 2a and so even this poorer fit is still very good.

It is not clear, therefore, if the underlying $\mathbf{L}^*_{Si}$ term should be $\exp(-t)$ or $1/t$ at this time. The ion intensities that we measure are a product of the neutral yield and the ionization probability. Indeed, the theory of Klushin et al. [37] for ionization probabilities shows that exponential and power law functions both occur and that, in general, both can operate but, under certain conditions, one of them can predominate. Indeed, the negative secondary ion yields of Ga_xAs_y clusters measured from GaAs by Goacher et al. [38] exhibit such a transition from exponential decays for the higher yielding cluster primary ions to a more power-like dependence for the lower yielding ions like Bi^+. Since the exponential function was a very close description for Si, the $\exp(-t)$ term will be used below for the rest of the analysis of Si.

The structure in $\mathbf{H}^*_{Si}$ should reflect the changes that may occur in either or both the neutral yield and the ionization probability for Si_t^+. The result of Figure 2b reflects the importance of the stability of the Si clusters. The number of Si_t neutrals is related to the binding energies of the different clusters. For Si, this varies more from cluster to cluster than is typical with most metals. The binding energy of different cluster sizes, at equilibrium, has been calculated in several publications [39–42] and, if these results are scaled against each other, the scatter is seen to be only 2%. The average result for the increased binding energy for each added atom, U', is shown together with $\mathbf{H}^*_{Si}$ by the solid square and round points, respectively, joined by the dotted line in Figure 3. Maxima $\mathbf{H}^*_{Si}$ at cluster sizes of 4, 6, and 10 are clearly observed. These maxima relate to specific structures with low-energy (high binding energy). If the increased binding energy, U', were the same as the bulk binding energy of 4.66 eV/atom, there would be no energy difference in sputtering a cluster compared with the same number of single atoms. It is the difference of the cluster binding energy from 4.66 eV/atom that defines how easily the clusters are formed. Where the difference is small, the cluster is more easily formed. Hence, the peaks in $\mathbf{H}^*_{Si}$ correlate with the peaks in U' at 4, 6, and 10 atoms and, in terms of the overall data in Figure 2a, the intensities have some similarities to thermal evaporation with contributions according to $\exp(-U_t/kT)$ where U_t is the energy required to remove the whole cluster and T is the effective average spike temperature, which is in the range 10,000 to 20,000 K. This is what is included in Urbassek's [31] gas expansion theory of sputtering. There, in his eq 11, the sputtering yield, Y, is given by

$$Y = Y_o\, t^{-a_n} \exp(-U_t/kT) \qquad (12)$$

where Y_o is a constant. Here we use a_n as a fitting parameter rather than the value of $2^{1/3}$ that Urbassek calculated.

Also shown in Figure 3 is the cluster Si spectrum, on a log intensity scale, formed by laser evaporation of Si quenched into cold He gas [43]. Here the spectrum only has data to $t = 11$ but peaks occur at 2 and 6 atoms with shoulders at 4 and 10 atoms. Finally, in Figure 3 is the mass spectrum for Ge clusters [44], for elemental vapor from a heated graphite source and again quenched into cooled He gas. Germanium has the same diamond lattice structure as silicon and should therefore show general similarities in the stable clusters [45]. This mass

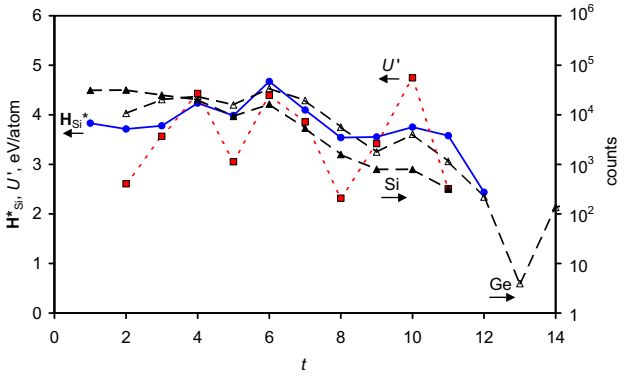

Figure 3. Values of $\mathbf{H}^*_{Si}$ from Figure (**2b**) (—•—) with the average added cluster binding energy, U' eV for the t^{th} Si atom (•••■•••). Also shown are the mass spectra of evaporated Si (--▲--) [43] and Ge (--△--) [44] on the intensity ordinate scale to the right.

spectrum is very similar to that for Si and shows the peaks at 4, 6, and 10 atoms as well as the rapid fall at higher t values. The fall with increasing t is slower than for Si since the binding energy of Ge, at 3.81 eV, is significantly lower than that at 4.66 eV for Si.

The correlation of the cluster structures and their stabilities in the emitted secondary ion intensity was seen, earlier, in the studies of alkali halides by Barlak et al. [34, 46]. There, stable, low-energy cubic-like $h \times k \times l$ filled structures were observed where h, k, and l were all odd-numbered values.

Figure 3 shows the clear relation of $\mathbf{H}^*_{Si}$ with the thermal mass spectra and the cluster binding energies. This is consistent with a thermal spike but does not preclude other mechanisms such as those of Urbassek [31] that also have dependence on the binding energies although in Urbassek's specific model, the atoms are either in a gaseous state or as a liquid close to the critical temperature that may preclude the manifestation of such structural aspects.

In the original derivation of eq 4 [12], secondary ion spectra for primary ions of different species were compared as well as for primary ions of different cluster sizes. In the study of Belykh et al. [19] of the sputtering of Si_t^+ secondary ion clusters, they also use Al_1^- and Al_2^- primary ions at 6, 9, 12, and 18 keV energy. The relative secondary ion yield data interestingly appear at first to be very different from those for Au_n^- shown in Figure 2a. They note that secondary ion mass peaks are only observed for $t \leq 4$ and that the sputtering of Si by light ions does not lead to the emission of large secondary cluster ions with $n > 4$. However, from our earlier study [12], we may expect that the secondary ion yields would again be described by $\mathbf{H}^*_{Si}$ as in Figure 2b and an exponential decay. Observations of Figure 2a and b would not indicate, immediately, a catastrophic event beyond $t = 4$.

Figure 4 shows the experimental data for the Al^- and Al_2^- primary ion data [19] as a function of t for the four energies by the open symbols. The fits to these data using eq 11 are shown by the small plotted points joined by dashed lines for Al^- and joined by solid lines for Al_2^-. The standard deviation of the fit is 4.7%, even better than in Figure 2a. The results are again described by eq 11 with the same $\mathbf{H}^*_{Si}$ as in Figure 2b, where the coefficients are given in Table 2. A sharp drop appears in Figure 4 at $t = 4$, down by a factor of 100 at $t = 5$ for 6 keV and around a factor of 20 for the other energies. The spectrum $\mathbf{H}^*_{Si}$, shown in Figure 2b, and the exponential decay form the two spectra for eq 11. These results, deduced for the Au_n^- primary ions, are seen to describe the data for Al_n^- primary ions above, very accurately. That the secondary ion spectra are formed as the product of a constant and two component spectra raised to appropriate powers, as found before for various primary ions for an organic solid [12], appears to be valid here for inorganic solids to a similar level of accuracy.

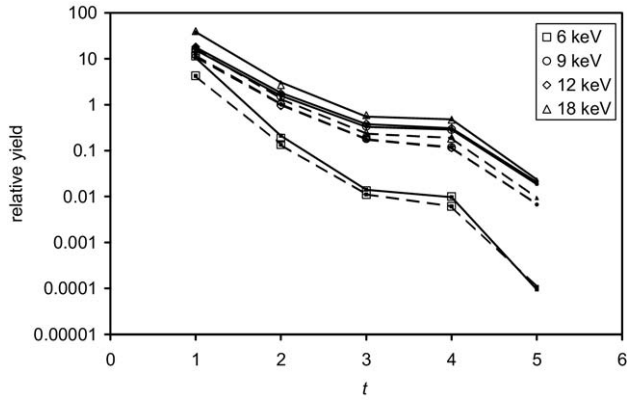

Figure 4. Data for the relative Si_t^+ secondary ion yields, normalized to the same Al_n^- primary ion currents, after Belykh et al. [19] for Al^-, dashed lines (---) and Al_2^-, solid lines (——) for (open square) 6 keV, (open circle) 9 keV, (open diamond) 12 keV, and (open triangle) 18 keV beam energies. The open symbols are the experimental data and the small points joined by the lines are the calculated results using eq 11.

Table 2. Values of parameters k_n and s_n for eq (11) for sputtering Si_t^+ by Al_n^- primary ions

Primary ion	Parameter	Energy, keV			
		6	9	12	18
Al^-	k_1	19.60	14.09	13.80	16.01
	s_1	2.84	2.01	1.99	2.04
Al_2^-	k_2	24.25	14.90	14.34	16.43
	s_2	3.14	1.83	1.83	2.01

The quality and consistency of data of Belykh et al. [19] may arise from the care with which the samples were treated before analysis. They heated the Si and sputtered with Au^- or Al^- primary ions until the SiO^+ secondary ion yield fell by two orders of magnitude to clean their samples in situ. Furthermore, their measurements were made at 1400 K to keep the prepared surface clean and so that defects in the crystal structure would be annealed. This is an excellent procedure but, importantly, may be different from the procedures used in the other work cited, which gives power law results. It is not known, now, if unannealed or unheated samples would give significantly different results.

Note that a significant difference between the results for Al_n^- and Au_n^- primary ions is that the parameter s_n falls as the energy rises for Au_n^- but goes through a minimum for Al_n^-. It is a reasonable approximation that the sputtering yield, Y, is related to the total ion yield and, if the latter is comprised of a series with intensities $\exp(-s_n t)$, then the parameter s_n is inversely related to Y. The sputtering yield for monatomic primary ions depends on the energy deposition density, dE/dx, at the surface. It is simple to show that the energy deposition density rises for Au^- in the energy range studied, but peaks for Al around 11–12 keV for normal incidence on Si [47]. This is more or less where the s_1 value is at minimum. The general behavior is thus consistent with the energy deposition at the surface. For cluster primary

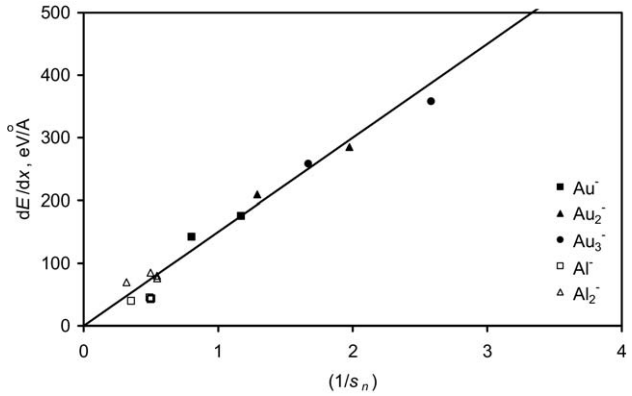

Figure 5. Data for $(1/s_n)$ from Tables 1 and 2, and the energy deposition rate dE/dx, calculated using SRIM 2006 [49] in eV/Å. The s_n values are calculated from the data of Belykh et al. [19] for Au_n^- and Al_n^- primary ions. The line shows a linear correlation.

ions of energy E_P, it is often assumed that the energy deposition rate is simply n times that for each of the atoms comprising the cluster at their individual energies E_P/n. This approximation is supported by the data of Andersen et al. [48] and so dE/dx is taken as $n d(E_P/n)/dx$.

Figure 5 shows the parameter $1/s_n$ from Tables 1 and 2 plotted versus the energy deposition rate calculated from SRIM 2006 [49] for primary ions of Au_n^- with $1 \leq n \leq 3$, and of Al_n^- with $1 \leq n \leq 2$. The correlation is very good indeed and indicates that the consideration of the parameters in Tables 1 and 2, to form a coherent dataset, is valid for the data from different ions, different energies, and different spectrometers. The correlation in Figure 5 is similar to, but rather more precise than, the earlier correlations of Morozov and Rasulev [18] for the sputtering of Ag, Nb, and Ta, and of Staudt and Wucher [28] for the sputtering of Ag, Al, Cu, Ge, Nb, and Ta, where b_n falls monotonically as the sputtering yield rises.

Conclusions

The sputtering of secondary ion clusters from inorganic solids by monatomic and cluster primary ions has been analyzed to test an earlier prediction from results for an organic solid [12] that the spectra (I_n) are formed from the product of a constant (F_n) and two sample-specific component spectra (**L*** and **H***) raised to powers (a_n and b_n) dependent on the primary ion cluster size, species and energy:

$$I_n = F_n (\mathbf{L}^*)^{a_n} (\mathbf{H}^*)^{b_n} \quad (13)$$

Results are presented for $(SiO_2)_tOH^-$ secondary ions sputtered from oxidized Si by Bi_n^- primary ions that show a correlation with the product of a spectrum $\mathbf{H}^*_{SiOH}$ and a simple power law spectrum raised to appropriate powers, within a standard deviation of 2.4% over 6 decades of intensity.

This test is then extended using published data for Si_t^+ secondary ions sputtered from Si by Au_n^- primary ions, and this shows a similarly good correlation with the product of a spectrum $\mathbf{H}^*_{Si}$ with, this time, a simple exponential spectrum both again being raised to appropriate powers. The spectrum $\mathbf{H}^*_{Si}$ is shown to reflect the stability of the Si clusters in a manner similar to mass spectrometry of the quenched vapor. It is confirmed that these two spectra can then be used directly to describe the cluster secondary ion intensities for the sputtering of Si_t^+ from Si using published data for Al_n^- primary ions. The main intensity contribution in the exponent of the exponential term is predicted to be related to the energy deposition rate. Data from SRIM 2006 shows that this is upheld for Au_n^- and Al_n^- primary ions of various energies.

This work does not prove that the underlying spectrum, **L***, is either exponential or power law, since good correlations may be made with both in different materials if appropriate **H*** spectra are used.

This work shows that results for different inorganic materials may be described, very accurately and coherently, as the product, here, of a constant and two component spectra, which depend on the secondary ions selected and the material sputtered, to powers that depend on the primary ion cluster size, species, and energy. This supports and broadens the earlier work for Irganox 1010, where similar conclusions were found [12].

Acknowledgments

This work forms part of the Chemical and Biological Program of the National Measurement System of the UK Department of Business, Innovation and Skills.

References

1. Gilmore, I. S.; Seah, M. P. Static SIMS: Towards Unfragmented Mass Spectra—The G-SIMS Procedure. *Appl. Surf. Sci.* **2000,** *161,* 465–480.
2. Gilmore, I. S.; Seah, M. P. G-SIMS of Crystallizable Organics. *Appl. Surf. Sci.* **2003,** *203/204,* 551–555.
3. Gilmore, I. S.; Seah, M. P. Organic Molecule Characterization—G-SIMS. *Appl. Surf. Sci.* **2004,** *231/232,* 224–229.
4. Gilmore, I. S.; Green, F. M.; Seah, M. P. G-SIMS-FPM: Molecular Structure at Surfaces—A Combined Positive and Negative Secondary Ion Study. *Appl. Surf. Sci.* **2006,** *252,* 6601–6604.
5. Green, F. M.; Gilmore, I. S.; Seah, M. P. G-SIMS and SMILES: Simulated Fragmentation Pathways for Identification of Complex Molecules, Amino Acids, and Peptides. *Appl. Surf. Sci.* **2008,** *255,* 852–855.
6. Green, F. M.; Dell, E. A.; Gilmore, I. S.; Seah, M. P. Identification of Complex Molecules at Surfaces: G-SIMS and SMILES Fragmentation Pathways. *Int. J. Mass Spectrom.* **2008,** *272,* 38–47.
7. Green, F. M.; Kollmer, F.; Niehuis, E.; Gilmore, I. S.; Seah, M. P. Imaging G-SIMS: A Novel Bismuth-Manganese Source Emitter. *Rapid Commun. Mass Spectrom.* **2008,** *22,* 2602–2608.
8. Seah, M. P.; Gilmore, I. S.; Green, F. M. G-SIMS: Relative Effectiveness of Different Monatomic Primary Ion Source Combinations. *Rapid Commun. Mass Spectrom.* **2009,** *23,* 599–602.
9. Vickerman, J. C.; Briggs, D.; Henderson, A., Eds; *The Static SIMS Library*, Version 4, SurfaceSpectra: Manchester, UK 2006; http://www.surfacespectra.com/simslibrary/index.html.
10. Schwede, B. C.; Heller, T.; Rading, D.; Niehius, E.; Wiedmann, L.; Benninghoven, A. *The Munster High Mass Resolution Static SIMS Library*, ION-TOF: Munster, 2003.
11. Briggs, D.; Brown, A.; Vickerman, J. C. *Handbook of Static Secondary Ion Mass Spectrometry (SIMS)*. Wiley: Chichester, 1989.
12. Seah, M. P.; Green, F. M.; Gilmore, I. S. Cluster Primary Ion Sputtering: Secondary Ion Intensities in Static SIMS of Organic Materials. *J. Phys. Chem. C*, unpublished.

13. Belykh, S. F.; Bitensky, I. S.; Mullajanov, D.; Rasulev, U. K. Nonlinear Effects in Cluster Emission from Solids Induced by Molecular Ion Impact. *Nucl. Instrum. Methods B* **1997,** *129,* 451–458.
14. Belykh, S. F.; Rasulev, U. K.; Samartsev, A. V.; Veryovkin, I. V. Comparative Study of Kinetic Energy Spectra and Mass Distributions of Ta_n^+ Ions Sputtered from Tantalum by Atomic and Molecular Ion Bombardment. *Nucl. Instrum. Methods B* **1998,** *136/138,* 773–778.
15. Belykh, S. F.; Rasulev, U. K.; Samartsev, A. V.; Verkhoturov, S. V.; Veryovkin, I. V. Sputtering of Tantalum by Atomic and Molecular Gold Ions: Comparative Study of Yields and Kinetic Energy Distributions of Atomic and Cluster Ions. *Microchim. Acta* **1998,** *15*(Suppl.), 379–385.
16. Belykh, S. F.; Habets, B.; Rasulev, U. K.; Samartsev, A. V.; Stroev, L. V.; Veryovkin, I. V. Relative Yields, Mass Distributions, and Energy Spectra of Cluster Ions Sputtered from Niobium Under keV Atomic and Polyatomic Gold Ion Bombardment. *Nucl. Instrum. Methods B* **2000,** *164/165,* 809–819.
17. Belykh, S. F.; Rasulev, U. K.; Samartsev, A. V.; Stroev, L. V.; Zinoviev, A. V. High Non-Additive Sputtering of Silicon as Large Positive Cluster Ions Under Polyatomic Ion Bombardment. *Vacuum* **2000,** *56,* 257–262.
18. Morozov, S. N.; Rasulev, U. K. Non-Additive Effects in Secondary-Ion Emission from V, Nb, and Ta Under Gold-Cluster Bombardment. *Appl. Surf. Sci.* **2004,** *231/232,* 78–81.
19. Belykh, S. F.; Kovarsky, A. P.; Palitsin, V. V.; Adriaens, A.; Adams, F. Non-Additive Sputtering of Silicon by keV Energy Molecular Projectiles of Heavy and Light Elements. *Int. J. Mass Spectrom.* **2001,** *209,* 141–152.
20. Baudin, K.; Brunelle, A.; Håkansson, P.; Le Beyec, Y.; Pautrat, M.; Pinho, R. R.; Schoppmann, Ch. Sputtering of Large Clusters from Solids Bombarded by High Energy Cluster Ions and Fullerenes. *Nucl. Instrum. Methods B* **1996,** *112,* 59–63.
21. Samartsev, A. V.; Wucher, A. Sputtering of Indium Using Polyatomic Particles. *Appl. Surf. Sci.* **2004,** *231/232,* 191–195.
22. Belykh, S. F.; Palitsin, V. V.; Adriaens, A.; Adams, F. Effect of Projectile Parameters on Charge State Formation of Sputtered Atoms. *Phys. Rev. B* **2002,** *66,* 195309.
23. Coon, S. R.; Calaway, W. F.; Pellin, M. J. Neutral Copper Cluster Sputtering Yields: Ne^+, Ar^+, and Xe^+ Bombardment. *Nucl. Instrum. Methods B* **1994,** *90,* 518–522.
24. Colla, Th. J.; Urbassek, H. M.; Wucher, A.; Staudt, C.; Heinrich, R.; Garrison, B. J.; Dandachi, C.; Betz, G. Experiment and Simulation of Cluster Emission from 5 keV Ar→Cu. *Nucl. Instrum Methods B* **1998,** *143,* 284–297.
25. Staudt, C.; Heinrich, R.; Wucher, A. Formation of Large Clusters During Sputtering of Silver. *Nucl. Instrum. Methods B* **2000,** *164/165,* 677–686.
26. Samartsev, A. V.; Wucher, A. Yields and Ionization Probabilities of Sputtered In_n Particles Under Atomic and Polyatomic Au_m^- Ion Bombardment. *Appl. Surf. Sci.* **2006,** *252,* 6474–6477.
27. King, B. V.; More, J. F.; Calaway, W. F.; Veyovkin, I. V.; Pellin, M. J. Sputtering of Clusters from Nickel-Aluminium. *Appl. Surf. Sci.* **2006,** *252,* 6426–6428.
28. Staudt, C.; Wucher, A. Generation of Large Indium Clusters by Sputtering. *Phys. Rev. B* **2002,** *66,* 075419.
29. Gilmore, I. S.; Seah, M. P. Ion Detection Efficiency in SIMS: Energy, Mass, and Composition Dependencies for Microchannel Plates Used in Mass Spectrometers. *Int. J. Mass Spectrom.* **2000,** *202,* 217–229.
30. Bitensky, I. S.; Parilis, E. S. Shock Wave Mechanism for Cluster Emission and Organic Molecule Desorption Under Heavy Ion Bombardment. *Nucl. Instrum. Methods B* **1987,** *21,* 26–36.
31. Urbassek, H. M. Sputtered Cluster Mass Distributions, Thermodynamic Equilibrium and Critical Phenomena. *Nucl. Instrum. Methods B* **1988,** *31,* 541–550.
32. Yamamoto, H.; Esaka, F.; Asakoka, H. Formation of Negative Carbon Cluster Ions by Molecular Ion Irradiation. *Proceedings of the SIMS XII*; Benninghoven, A.; Bertrand, P.; Migeon, H. N.; Werner, H. W., Eds. Elsevier: Amsterdam, 2000; pp 295–298.
33. Brunelle, A.; Della-Negra, S.; Depauw, J.; Jacquet, D.; Le Beyec, Y.; Putrat, M.; Baudin, K.; Andersen, H. H. Enhanced Secondary-Ion Emission Under Gold-Cluster Bombardment with Energies from keV to MeV Per Atom. *Phys. Rev. A* **2001,** *63,* 022902.
34. Barlak, T. M.; Campana, J. E.; Colton, R. J.; DeCorpo, J. J.; Wyatt, J. R. Secondary Ion Mass Spectrometry of Metal Halides. 1. Stability of Alkali Iodide Clusters. *J. Phys. Chem.* **1981,** *85,* 3840–3844.
35. Barlak, T. M.; Campana, J. E.; Wyatt, J. R.; Colton, R. J. Secondary Ion Mass Spectrometry of Metal Halides. 3. Ionic Radii Effects in Alkali Halide Clusters. *J. Phys. Chem.* **1983,** *87,* 3441–3445.
36. Gilmore, I. S.; Seah, M. P. Static SIMS: A Study of Damage Using Polymers. *Surf. Interface Anal.* **1996,** *24,* 746–762.
37. Klushin, D. V.; Gusev, M. Yu.; Urazgil'din, I. F. Velocity Dependence of Ionization Probability of Secondary Ions Emitted from Metal Surfaces. *Nucl. Instrum. Methods B* **1995,** *100,* 316–321.
38. Goacher, R. E.; Luo, H.; Gardella, J. A. Formation of High-Mass Cluster Ions from Compound Semiconductors Using Time-of-Flight Secondary Ion Mass Spectrometry with Cluster Primary Ions. *Anal. Chem.* **2008,** *80,* 3261–3269.
39. Raghavachari, K.; Logovinsky, V. Structure and Bonding in Small Silicon Clusters. *Phys. Rev. Lett.* **1985,** *55,* 2853–2856.
40. Raghavachari, K. Theoretical Study of Small Silicon Clusters: Equilibrium Geometries and Electronic Structures of Si_n (n = 2–7, 10), *J. Chem. Phys.* **1986,** *84,* 5672–5686.
41. Raghavachari, K.; Rohfling, C. M. Bonding and Stabilities of Small Silicon Clusters: A Theoretical Study of Si_7–Si_{10}. *J. Chem. Phys.* **1988,** *89,* 2219–2234.
42. Zhu, X.; Zeng, X. C. Structures and Stabilities of Small Silicon Clusters: Ab Initio Molecular-Orbital Calculations of Si_7–Si_{11}. *J. Chem. Phys.* **2003,** *118,* 3558–3570.
43. Maruyama, S.; Kinbara, H.; Hayashi, H.; Kimura, D. Photoionized TOF Mass Spectrometry of Atomic Clusters. *Microscale Thermophysical Engineering* **1997,** *1,* 39–46.
44. Martin, T. P.; Schaber, H. Mass Spectra of Si, Ge, and Sn clusters. *J. Chem. Phys.* **1985,** *83,* 855–858.
45. Honig, R. E. Sublimation Studies of Silicon in the Mass Spectrometer. *J. Chem. Phys.* **1954,** *22,* 1610–1611.
46. Barlak, T. M.; Campana, J. E.; Wyatt, J. R.; Dunlap, B. I.; Colton, R. J. Secondary Ion Mass Spectrometry of Metal Salts: Polyatomic Ion Emission. *Int. J. Mass Spectom.* **1983,** *46,* 523–526.
47. Seah, M. P.; Clifford, C. A.; Green, F. M.; Gilmore, I. S. An Accurate Semi-Empirical Equation for Sputtering Yields, I: for Argon Ions. *Surf. Interface Anal.* **2005,** *37,* 444–458.
48. Andersen, H. H.; Johansen, A.; Olsen, M.; Touboltzev, V. Gold-Cluster Ranges in Aluminium, Silicon, and Copper. *Nucl. Instrum. Methods B* **2003,** *212,* 56–62.
49. SRIM 2006 *The Stopping and Range of Ions in Matter*, available for download from http://www.SRIM.org.